COMMUNICATION

Check for updates

Neutral rhodol-based dyes expressing localization in mitochondria†

Ilaria Ferraboschi, ‡[a] Juraj Ovčar,‡[b,c] Kateryna V. Vygranenko,[d] Shupei Yu,[e] Alfonso Minervino,[e] Antoni Wrzosek,[f] Adam Szewczyk,[f] Riccardo Rozza,[c] Alessandra Magistrato,[c] Kevin D. Belfield,[e] Daniel T. Gryko,[d] Luca Grisanti *[b,c] and Cristina Sissa *[a]

Neutral rhodol-based red emitters are shown to efficiently localize in mitochondria, as demonstrated by confocal microscopy and co-localization studies. A simple model is proposed to explain the localization mechanism of neutral molecules. The model takes into account the strong coupling between the molecular dipole moment and the electric field of the inner mitochondrial membrane.

Mitochondria are organelles found in the cytoplasm of most eukaryotic cells. Mitochondrial dysfunction has been shown to have far-reaching consequences, being implicated as a major contributing factor in the development of various diseases.[1] Monitoring mitochondrial morphology and dynamics *via* fluorescent probes (trackers) can reveal valuable information on cell functioning,[2] allowing for the development of disease treatment strategies based on understanding mitochondrial dysfunction and its pathological implications at the molecular level.[3]

The vast majority of commercially available mitochondria trackers are positively charged,[4–6] exploiting the electro-chemical potential difference $\Delta\mu_{H^+}$ generated across the mitochondrial inner membrane as a result of a proton gradient established by the respiratory chain.[7] In contrast to cationic trackers, there have been far fewer reports of neutral tracking probes[5,8–17] despite several significant advantages neutral trackers offer over charged ones; *e.g.*, their accumulation in mitochondria does not lead to membrane depolarization,[13,15] allowing for the investigation of mitochondrial morphology in a minimally perturbed environment. The efficiency of cationic trackers is heavily dependent on the mitochondrial membrane potential,[5,18] leading to an inability to label dysfunctional mitochondria[18] or mitochondria with membrane potentials temporarily altered by normal biological processes.[18,19] It has been shown that common cationic trackers may stain organelles other than mitochondria, such as lysosomes, due to their own membrane potential.[19,20] It is also known that the mitochondrial inner membranes intrinsically possess low ion permeability,[21,22] requiring additional considerations in the design of cationic trackers.

Generally, the physical mechanisms of the localization of neutral molecules in mitochondria are not fully understood. The lack of understanding of the physical processes underpinning mitochondrial localization of neutral trackers from a fundamental point of view is detrimental to the formulation of improved strategies for rational design of novel trackers, as well as to the integrity of the interpretations of mitochondrial tracking experiments.

In this paper, by performing confocal microscopy experiments and co-localization studies with a commercial mitochondrial tracker, we demonstrate that the red-fluorescent rhodol-based dyes **FM** and **MOFM** (Fig. 1) function as efficient neutral mitochondral trackers. In addition, we propose a physical mechanism governing mitochondrial localization of neutral polar molecules.

FM and **MOFM** were previously synthesized by some of us as efficient red emitters.[23] The two molecules share the same sulfone-rhodol backbone, while the substituted upper ring confers stability. Based on density functional theory (DFT)

[a]Department of Chemistry, Life Sciences and Environmental Sustainability, University of Parma, 43124 Parma, Italy. E-mail: cristina.sissa@unipr.it
[b]Ruđer Bošković Institute, Bijenička cesta 54, 10000 Zagreb, Croatia. E-mail: grisanti@iom.cnr.it
[c]National Research Council – Materials Foundry Institute (CNR-IOM) c/o SISSA (International School for Advanced Studies), Via Bonomea 265, 34136 Trieste, Italy
[d]Institute of Organic Chemistry, Polish Academy of Sciences, Kasprzaka 44/52, 01-224 Warsaw, Poland
[e]Department of Chemistry and Environmental Science, College of Science and Liberal Arts, New Jersey Institute of Technology, Newark, New Jersey 07102, USA
[f]Nencki Institute of Experimental Biology of Polish Academy of Sciences, Pasteura 3, 02-093 Warsaw, Poland

5886 | *Org. Biomol. Chem.*, 2024, **22**, 5886–5890

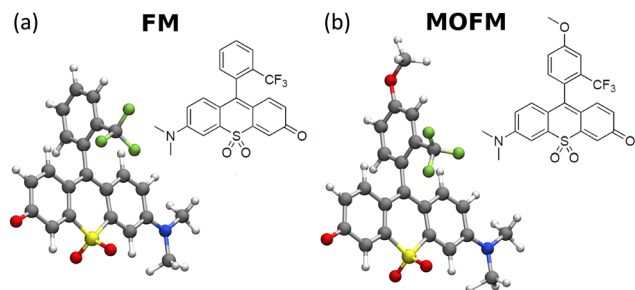This journal is © The Royal Society of Chemistry 2024

Fig. 1 Chemical structures and ground state geometries obtained by DFT of (a) **FM** and (b) **MOFM**.

simulations (computational details reported in sect. S1†), the two aromatic groups are almost perpendicular to each other (see Fig. 1 and Tables S2 and S3†), suggesting negligible conjugation between the two units. Spectroscopic characterization was already available,[23] and here it is extended to include cell culture medium and PBS (Fig. S5; technical details in sect. S2†). The results show a marked positive solvatochromism, suggesting that (i) both the ground and the first excited states are polar, (ii) the permanent dipole moment of the first excited state is larger than the ground state dipole moment, and (iii) the low-energy transition has a charge transfer character.

The excitation anisotropy of **FM** and **MOFM** in glycerol (Fig. S6†) has a constant value of 0.4 within the broad excitation band, confirming that only one excited state is involved in this transition and that the same excited state is responsible for absorption and emission. To further investigate excited states of **FM** and **MOFM**, we measured two-photon absorption (2PA) spectra in DCM (Fig. S7†). 2PA spectra of both compounds overlap very well with one-photon absorption which is a further confirmation of their dipolar nature.[24] They exhibit similar values of the 2PA cross section σ ($\sigma_{\mathbf{FM}}^{\lambda_{\max}}$ = 120 GM and $\sigma_{\mathbf{MOFM}}^{\lambda_{\max}}$ = 110 GM), showing that both molecules are suitable candidates for two-photon microscopy experiments.

DFT and time-dependent density functional theory (TDDFT) simulations in implicit solvents provide important information on the orientation of dipole moments (Tables S2 and S3†): the transition dipole moment from the ground state S_0 to the first excited state S_1 is oriented along the long axis of the 3-ring moieties, while the ground-state dipole moment forms an angle of approximately 30° with respect to it. TDDFT results (Tables S4 and S5†) correctly reproduce the experimental solvatochromism with a bright first transition (with a HOMO–LUMO dominance; see molecular orbitals in Fig. S3 and S4†), while $S_0 \rightarrow S_2$ appears to be a dark transition with a $n \rightarrow \pi^*$ character. Interestingly, the behaviour is different in vacuum and S_1 and S_2 are reversed.

To assess the propensity of the compounds to selectively localize in mitochondria, we conducted experiments on HeLa cells stained with **FM** and **MOFM**. Measurements of cell viability (Fig. S9†) after 24 hours of incubation show that the compounds become toxic for the cells at concentrations above

1 μM. In order to reduce the effect of toxicity in further experiments, we performed measurements after incubating cells for 30 min using a concentration of 1.5 μM. Owing to the excellent optical properties of both **FM** and **MOFM** in terms of fluorescence quantum yield and molar extinction coefficient, the effects of toxicity can be mitigated by keeping the concentration at 1 μM or lower and adjusting the excitation power and/or detector gains to maintain high quality images. Images of HeLa cells stained with **FM** and **MOFM** (Fig. S10†) confirm the uptake of dyes, as is further evidenced by the red emission from the incubated cells (Fig. S8†). The images of HeLa cells incubated with **FM** and **MOFM** indicate that the dyes localize in some organelles. Therefore, we investigated co-localization of **FM** and **MOFM** with MitoTracker™ Green[25] (MTG), a commercially available dye (Fig. 2). The Pearson correlation coefficients (PCCs), calculated from the resulting images, are $PCC_{\mathbf{FM}}$ = 0.79 and $PCC_{\mathbf{MOFM}}$ = 0.89, showing that both compounds selectively localize inside mitochondria, with **MOFM** having a stronger localization tendency compared to **FM**. While the PCC of **MOFM** is so high that we deem co-localization experiments in other organelles unnecessary, for **FM** we investigated possible localization in lysosomes by performing a co-localization experiment of **FM** and Lysotracker Green (Fig. S11†): the resulting PCC is 0.6, confirming a low degree localization within these organelles.

While for cationic trackers the physical localization mechanism is well understood, reports of neutral mitochondrial trackers often remain unclear or silent on their localization mechanism (sect. S5 and S6†). Here we propose a mechanism based on the electrostatic interaction between a neutral polar molecule and the inner mitochondrial membrane. A discussion of further reasonable mitochondrial localization mechanisms for neutral molecules is given in sect. S6;† however, we determined that they do not apply to the dyes presented in this work.
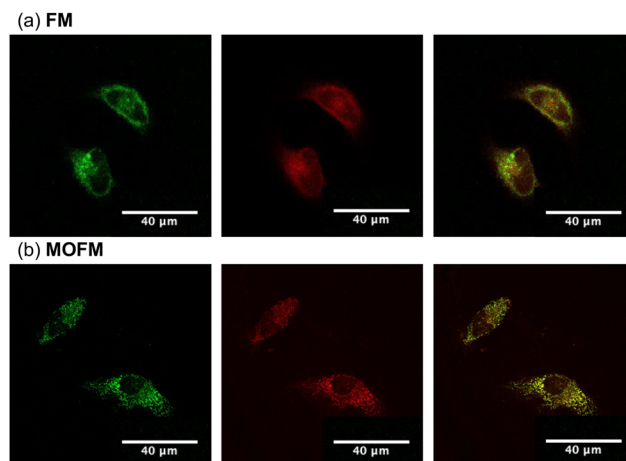

Fig. 2 Co-localization of (a) **FM** and (b) **MOFM** with MTG in HeLa cells. The left panels show images of MTG, the middle panels show images of **FM** and **MOFM** respectively, with the merged images being shown on the right panels. Scale bar: 40 μm.

The interior of the inner mitochondrial membrane can be modeled as a phospholipid bilayer of palmitoyl-oleyl-phosphatidylcholine (POPC), while the intermembrane space and the mitochondrial matrix are considered aqueous solutions.[26–28] The total electrostatic potential of a one-dimensional inner mitochondrial membrane is then given by:

$$\Phi(x, \Delta\Psi_{NP}) = \Phi_P(x, \Delta\Psi_{NP}) + \Phi_W(x, \Delta\Psi_{NP}) \quad (1)$$

where Φ_P is the electrostatic potential generated by the POPC bilayer, Φ_W is generated by water and $\Delta\Psi_{NP}$ is the voltage drop across the membrane induced by a homogeneous electric field, stemming from the proton gradient established during the Krebs cycle. To fit a functional form of Φ, we utilize results from molecular dynamics (MD) simulations of the water-POPC bilayer system.[29] We set the origin ($x = 0$) to be at the center of the POPC bilayer, with the intermembrane space being located in the $-\hat{x}$ direction from the phospholipid bilayer (i.e. $x \to -\infty$) and the mitochondrial matrix being located in the $+\hat{x}$ direction ($x \to +\infty$). The obtained fitted curves are shown on Fig. S12,† with the explicit functional forms and the fitted parameters given in sect. S7.†

As can be seen from Fig. S13,† the calculated electric field across the membrane indeed exhibits significant variation on the length scale of **FM** and **MOFM** (≈ 10 Å), allowing for a net electrostatic force on the polar molecules. We consider a model in which we represent a molecule as a collection of N rigidly connected particles with respective masses m_i and partial charges q_i. The equations of motion for these particles in a spatially varying one-dimensional electric field $\vec{E}(x) = E(x)\hat{x}$ are:

$$m_i\ddot{x}_i = q_i E(x_i) \quad (2)$$

where x_i is the x-component of the position of particle i. Introducing a coordinate for the center of mass of the molecule as X, we can sum the equations of motion (2) to obtain:

$$M\ddot{X} = \sum_i^N q_i E(X + l_i) \quad (3)$$

where M is the mass of the molecule and $l_i = x_i - X$. Therefore, the net force experienced by the polar molecule is $F(X) = \sum_i^N q_i E(X + l_i)$.

In a stationary state, the molecule will be oriented in such a way that the dipole moment $\vec{\mu}$ is aligned with $\vec{E}(x)$. Let us fix $\{l_1...l_N\}$, so that the dipole moment is parallel to the x-axis, i.e. $\vec{\mu} = \mu\hat{x}$. Then, the respective electrostatic potential energies $E_p^{\pm}(x)$ for the two configurations with the dipole moment being (anti)parallel to the x-axis are simply:

$$E_p^{\pm}(x) = -\int_{-\infty}^{x} F(x' \pm l_i)dx' = \sum_i^N q_i \Phi(x \pm l_i) \quad (4)$$

Note that x in eqn (4) denotes the position of the molecular center of mass. To obtain the ionic point charges q_i, we calculate Mulliken charges from the ground state electronic density obtained by DFT optimizations of **FM** and **MOFM** in vacuum and water. We test different environments as it is not trivial to determine which is the most representative environment of the relevant realistic physical system.[30] It is known that the center of the inner mitochondrial membrane is non-polar, with the value of the relative permittivity being $\varepsilon \approx 2$, while the relative permittivity of the aqueous solutions representing the intermembrane space and the mitochondrial matrix is $\varepsilon \approx 80$.[28,30,31]

From Table 1, we can see that the dipole moments calculated using Mulliken charges agree well with the dipole moments calculated directly from the electronic density obtained using DFT. Furthermore, we note that both molecules have large dipole moments and are highly polarizable. The large dipole moment is a result of donor and acceptor groups connected at the two ends of the conjugated molecular unit, similarly to push–pull molecules.

The electrostatic potential energies calculated as per eqn (4), using Mulliken charges obtained in different solvents and using $\Delta\Psi_{NP} = -0.15$ V, are shown on Fig. 3, with the binding energies $E_b^{\pm}$ (minimal values of $E_p^{\pm}(x)$) being listed in Table 1. We find that two binding sites at $x \approx \pm 16$ Å exist for both **FM** and **MOFM**. These positions are found within the phospholipid bilayer, as the lipid heads are located at $x \approx \pm 20$ Å.[29] Both binding sites are stable with respect to molecular rotations (Fig. S14†). From Table 1, we observe that the binding energy of the site near the mitochondrial matrix (E_b^+) is consistently lower than the one of the site near the intermembrane space (E_b^-). This asymmetry in the binding energies between the two sites stems from the polarization of the POPC and water subsystems due to $\Delta\Psi_{NP}$. Notably, we find that all calculated binding energies for **MOFM** are lower than the corresponding ones for **FM**, consistent with the experimental observation that **MOFM** has a larger tendency to localize in mitochondria compared to **FM**. Because of the difficulty in determining the most appropriate ionic charges (see discussion above), we consider the binding energies calculated using Mulliken charges obtained in vacuum (water) to represent the upper (lower) bound of the real electrostatic binding energy; however, we note that, due to the large solvatochromism of the considered molecules, the similarity in the measured emission spectra of **MOFM** in PBS ($\varepsilon \approx 79$) and cells (Fig. S8†) indicates that the relevant physical environment could be best approximated by water.

Table 1 Ground state dipole moments (in Debye) of **FM** and **MOFM** in different solvents, calculated using the electronic density obtained with DFT (μ_ρ) and Mulliken charges (μ_M); electrostatic binding energies (in meV), calculated using Mulliken charges obtained in different solvents for dipole moments parallel (E_b^+) and antiparallel (E_b^-) to the x-axis

Molecule	Solvent	μ_ρ	μ_M	E_b^+	E_b^-
FM	Vacuum	12.346	13.253	−347	−326
	Water	22.918	23.084	−598	−561
MOFM	Vacuum	12.638	13.716	−353	−332
	Water	23.211	23.492	−606	−570

5888 | Org. Biomol. Chem., 2024, **22**, 5886–5890

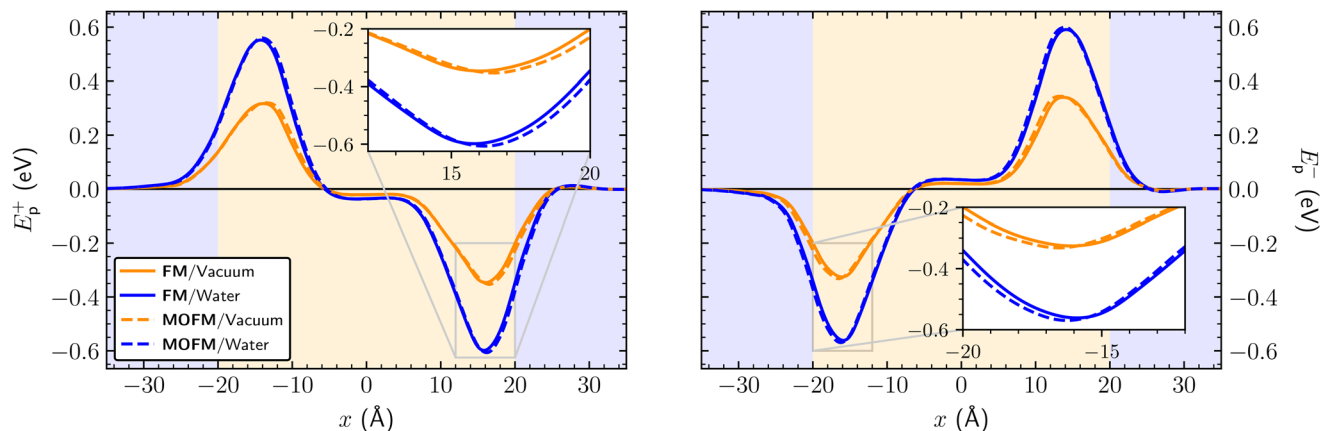This journal is © The Royal Society of Chemistry 2024

Fig. 3 Electrostatic potential energy across the inner mitochondrial membrane as a function of the position of the molecular center of mass, calculated using Mulliken charges in different solvents (vacuum and water) for dipole moments parallel (left panel) and antiparallel (right panel) to the x-axis. The binding sites (see text) are shown magnified in the insets. The region containing predominantly water (POPC) is highlighted by the light blue (orange) background. The voltage drop across the membrane was set to $\Delta\Psi_{NP} = -0.15$ V.

To calculate the total binding energy, it is necessary to account for all molecule–membrane interactions other than the electrostatic one (*e.g.* hydrophobic, van der Waals, steric and specific chemical interactions). This is difficult to achieve without the use of more complex methods, *i.e.*, a detailed study of molecular permeation through the inner mitochondrial membrane. We elect to leave this task to a future investigation and instead offer a qualitative assessment of the aforementioned factors. Using a simple lipophilicity model,[32] we obtain $\log P = 3$ for both **FM** and **MOFM**, meaning that both molecules are significantly hydrophobic. This further enhances localization to the POPC bilayer.[27,28] Steric and other factors have been shown to be of secondary importance in modeling hydrophobic ion interactions with membranes[30] and are unlikely to hinder localization within the POPC bilayer, especially considering the large electrostatic binding energy, high lipophilicity and the comparatively small size of **FM** and **MOFM** with respect to some of the larger lipophilic mitochondria trackers.[4–6]

Finally, we estimated the ratio of the concentrations of **FM** and **MOFM** localized in mitochondria. Due to the structural similarity of the considered molecules, we assume that the total binding energies of the two molecules significantly differ only in the electrostatic contribution. We can then use the following expression to approximate the ratio of concentrations of localized molecules:

$$\gamma = \frac{e^{-\beta E_{b,FM}^{+}} + e^{-\beta E_{b,FM}^{-}}}{e^{-\beta E_{b,MOFM}^{+}} + e^{-\beta E_{b,MOFM}^{-}}} \qquad (5)$$

where we calculate the thermodynamic β parameter using a temperature of 36 °C. The values of γ, calculated using Mulliken charges obtained in vacuum and water are respectively 0.78 and 0.73, comparable to the ratio of the measured Pearson correlation coefficients ($PCC_{FM}/PCC_{MOFM} \approx 0.89$), which can also be interpreted as an approximation to the ratio

of concentrations of localized molecules, showing that our model is quantitatively sound.

To further deepen our investigation, a computational investigation of a more specific localization scenario was attempted (sect. S8†). In general, the possibility that these dyes, once in the inner mitochondrial space, interact with specific sites (proteins) may deserve further investigations.

In this work, we reported on new red emitter neutral mitochondrial trackers constituted by substituted rhodol-based structures. Both **FM** and **MOFM** show specific mitochondrial localization, co-localizing with MTG to a very high degree, comparable to both cationic[33,34] and neutral[14] novel mitochondrial trackers. Moreover, **FM** and **MOFM** are red emitters that exhibit high fluorescence quantum yields and large extinction coefficients. This makes them suitable for use as fluorescent probes in bio-imaging at very low concentrations.[23]

Our combined experimental and computational study made it possible to suggest that the electrostatic interaction between molecular dipole moment and the electric field present at the inner mitochondrial membrane is responsible for the selective localization mechanism. By providing a straightforward and physically transparent model for the localization mechanism, we have made a significant step forward towards rational design of novel neutral mitochondrial trackers and understanding their localization in mitochondria.

Conflicts of interest

There are no conflicts to declare.

Acknowledgements

This journal is © The Royal Society of Chemistry 2024

Org. Biomol. Chem., 2024, **22**, 5886–5890 | **5889**

References

1 Y. Li, Y. Ma, Q.-Y. Dang, X.-R. Fan, C.-T. Han, S.-Z. Xu and P.-Y. Li, *Life Sci.*, 2022, **306**, 120834.

2 M. Karbowski and R. Youle, *Cell Death Differ.*, 2003, **10**, 870–880.

3 S. R. Pieczenik and J. Neustadt, *Exp. Mol. Pathol.*, 2007, **83**, 84–92.

4 H. Crawford, M. Dimitriadi, J. Bassin, M. T. Cook, T. F. Abelha and J. Calvo-Castro, *Chem. – Eur. J.*, 2022, **28**, e202202366.

5 B. A. Neto, J. R. Corrêa and R. G. Silva, *RSC Adv.*, 2013, **3**, 5291–5301.

6 X. Zhang, Q. Sun, Z. Huang, L. Huang and Y. Xiao, *J. Mater. Chem. B*, 2019, **7**, 2749–2758.

7 D. G. Nicholls, *Essays Biochem.*, 2010, **47**, 25–35.

8 J. Jose, A. Loudet, Y. Ueno, R. Barhoumi, R. C. Burghardt and K. Burgess, *Org. Biomol. Chem.*, 2010, **8**, 2052–2059.

9 B. A. D. Neto, J. R. Corrêa, P. H. Carvalho, D. C. Santos, B. C. Guido, C. C. Gatto, H. C. de Oliveira, M. Fasciotti, M. N. Eberlin and E. N. d. Silva Jr, *J. Braz. Chem. Soc.*, 2012, **23**, 770–781.

10 T. Gayathri, S. Karnewar, S. Kotamraju and S. P. Singh, *ACS Med. Chem. Lett.*, 2018, **9**, 618–622.

11 H. Yao, G. Wei, Y. Liu, H. Yao, Z. Zhu, W. Ye, X. Wu, J. Xu and S. Xu, *ACS Med. Chem. Lett.*, 2018, **9**, 1030–1034.

12 P. E. Kesavan, V. Pandey, M. K. Raza, S. Mori and I. Gupta, *Bioorg. Chem.*, 2019, **91**, 103139.

13 Y. Wang, B. Xu, R. Sun, Y.-J. Xu and J.-F. Ge, *J. Mater. Chem. B*, 2020, **8**, 7466–7474.

14 Á. Ramos-Torres, E. Avellanal-Zaballa, F. García-Garrido, A. B. Fernández-Martínez, A. Prieto-Castaneda, A. R. Agarrabeitia, J. Bañuelos, I. García-Moreno, F.-J. Lucio-Cazana and M. J. Ortiz, *Chem. Commun.*, 2021, **57**, 5318–5321.

15 W. Ma, B. Xu, R. Sun, Y.-J. Xu and J.-F. Ge, *J. Mater. Chem. B*, 2021, **9**, 2524–2531.

16 B. Roy, M. C. Reddy, G. P. Jose, F. C. Niemeyer, J. Voskuhl and P. Hazra, *J. Phys. Chem. Lett.*, 2021, **12**, 1162–1168.

17 H. G. Agrawal, P. S. Giri, P. Meena, S. N. Rath and A. K. Mishra, *ACS Med. Chem. Lett.*, 2023, **14**, 1857–1862.

18 K. Neikirk, A. G. Marshall, B. Kula, N. Smith, S. LeBlanc and A. Hinton Jr, *Eur. J. Cell Biol.*, 2023, **102**, 151371.

19 F. Dong, M. Zhu, F. Zheng and C. Fu, *FEBS J.*, 2022, **289**, 262–278.

20 P. E. Klier, R. Roo and E. W. Miller, *Curr. Opin. Chem. Biol.*, 2022, **71**, 102203.

21 P. Bernardi, *Physiol. Rev.*, 1999, **79**, 1127–1155.

22 J. J. Lemasters, *J. Gastroenterol. Hepatol.*, 2007, **22**, S31–S37.

23 K. V. Vygranenko, Y. M. Poronik, A. Wrzosek, A. Szewczyk and D. T. Gryko, *Chem. Commun.*, 2021, **57**, 7782–7785.

24 F. Terenziani, C. Katan, E. Badaeva, S. Tretiak and M. Blanchard-Desce, *Adv. Mater.*, 2008, **20**, 4641–4678.

25 A. D. Presley, K. M. Fuller and E. A. Arriaga, *J. Chromatogr. B: Anal. Technol. Biomed. Life Sci.*, 2003, **793**, 141–150.

26 B. Ketterer, B. Neumcke and P. Läuger, *J. Membr. Biol.*, 1971, **5**, 225–245.

27 R. F. Flewelling and W. L. Hubbell, *Biophys. J.*, 1986, **49**, 531–540.

28 M. F. Ross, G. Kelso, F. H. Blaikie, A. M. James, H. M. Cocheme, A. Filipovska, T. Da Ros, T. Hurd, R. A. Smith and M. P. Murphy, *Biochemistry (Moscow)*, 2005, **70**, 222–230.

29 L. Delemotte and M. Tarek, *J. Membr. Biol.*, 2012, **245**, 531–543.

30 R. F. Flewelling and W. L. Hubbell, *Biophys. J.*, 1986, **49**, 541–552.

31 B. H. Honig, W. L. Hubbell and R. F. Flewelling, *Annu. Rev. Biophys. Biophys. Chem.*, 1986, **15**, 163–193.

32 R. Mannhold, G. I. Poda, C. Ostermann and I. V. Tetko, *J. Pharm. Sci.*, 2009, **98**, 861–893.

33 X. Song, N. Li, C. Wang and Y. Xiao, *J. Mater. Chem. B*, 2017, **5**, 360–368.

34 T. Gao, H. He, R. Huang, M. Zheng, F.-F. Wang, Y.-J. Hu, F.-L. Jiang and Y. Liu, *Dyes Pigm.*, 2017, **141**, 530–535.

5890 | *Org. Biomol. Chem.*, 2024, **22**, 5886–5890

This journal is © The Royal Society of Chemistry 2024